Mechanistic Studies of Improved Foam EOR Processes

Semi-Annual Report for the Period
September 1, 2003 – February 29, 2004

Principal Author:

William R. Rossen

Date Report Issued: June 14, 2004

Work Performed under Contract DE-FC26-01BC15318

The University of Texas at Austin
Center for Petroleum and Geosystems Engineering
1 University Station, C0300
Austin, TX 78712-1061

DISCLAIMER

Mechanistic Studies of Improved Foam EOR Processes

Contract No. DE-FC26-01BC15318

The University of Texas at Austin
1 University Station, C0300
Austin, TX 78712-1061

Contract Date: Sept. 1, 2001
Anticipated Completion: Aug. 31, 2004

ABSTRACT

The objective of this research is to widen the application of foam to enhanced oil recovery (EOR) by investigating fundamental mechanisms of foams in porous media. This research will lay the groundwork for more applied research on foams for improved sweep efficiency in miscible gas, steam and surfactant-based EOR. Task 1 investigates the pore-scale interactions between foam bubbles and polymer molecules. Task 2 examines the mechanisms of gas trapping, and interaction between gas trapping and foam effectiveness. Task 3 investigates mechanisms of foam generation in porous media.

Significant progress was made during this period on all three Tasks.

Regarding Task 1, we continued comparisons of foam behavior in sandpacks with and without polymer and oil. As in our previous results, decane was moderately destabilizing to foam. Xanthan polymer did not stabilize foam in the presence of decane in this case. Rather, it appears to have destabilized foam, so that pressure gradient decreased in spite of the increase in aqueous-phase viscosity.

Research on Task 2 included the first shake-down experiments with our new apparatus for gas-phase tracer tests for direct measurement of trapped-gas saturation with foam. In addition, we began to analyze CT images of gas-phase tracer in foam displacements, which offers an independent measure of trapped-gas fraction and insights into the roles of convection of tracer in flowing gas and diffusion into trapped gas.

Research on Task 3 included foam generation experiments in heterogeneous sandpacks and beadpacks and modeling of discontinuous changes in state such as foam generation. The experiments found the same three regimes (coarse foam, strong foam, and intermediate regime) in heterogeneous sandpacks previously identified in homogeneous porous media. One implication is that there may be a minimum flow rate required for foam generation in even heterogeneous porous media. The dynamics in SAG foam processes in heterogeneous media are complex. When a given pressure drop is imposed, a pressure wave moves down the pack. Foam may nearly plug the pack at a transition in permeability, but it is still important whether the foam thus formed propagates further or remains in place.

Modeling of discontinuous changes in state such as foam generation shows that these changes can be accommodated within the framework of fractional-flow theory. Fractional-flow theory has the advantage that it does not suffer from the artifacts of

coarse gridding often seen in conventional simulation. Our modeling shows that it can be crucial whether the formation of strong foam affects the capillary-pressure function for the porous medium. If it does, this may lead to a new foam bank in a SAG displacement not predicted without accounting for this effect.

This period saw the publication of one article in a refereed journal:

Kam, S. I., and Rossen, W. R., "A Model for Foam Generation in Homogeneous Porous Media," *SPE Journal* **8** (Dec. 2003), 417-425.

one more accepted for publication:

Rossen, W.R., and van Duijn, C.J., "Gravity Segregation in Steady-State Horizontal Flow in Homogeneous Reservoirs," accepted by *J. Petr. Sci. Eng.*

and two manuscripts prepared for presentation at technical conferences:

Kim, J. S., Dong., Y., and Rossen, W. R., "Steady-State Flow Behavior of CO_2 Foam," SPE 89351 presented at the 2004 SPE/DOE Symposium on Improved Oil Recovery, Tulsa, OK, 17-21 April.

Rossen, W. R., and Bruining, J., "Foam Displacements With Multiple Steady States," SPE 89397 presented at the 2004 SPE/DOE Symposium on Improved Oil Recovery, Tulsa, OK, 17-21 April.

TABLE OF CONTENTS

OBJECTIVES

The objective of this research is to widen the application of foam to enhanced oil recovery (EOR) by investigating fundamental mechanisms of foams in porous media. This research will lay the groundwork for more applied research on foams for improved sweep efficiency in miscible gas, steam and surfactant-based EOR. Task 1 investigates the pore-scale interactions between foam bubbles and polymer molecules. Task 2 examines the mechanisms of gas trapping, and interaction between gas trapping and foam effectiveness. Task 3 investigates mechanisms of foam generation in porous media.

EXPERIMENTAL

The experimental techniques employed vary with the specific task addressed. Therefore the experimental techniques are discussed together with the Results and Discussion section on each task, below.

RESULTS AND DISCUSSION

TASK 1: INTERACTIONS BETWEEN POLYMER AND FOAM

This work is motivated by a hypothesis about how polymer interacts with foam in porous media. The hypothesis derives in turn from the observation that steady-state foam behavior appears to comprise two very different flow regimes, at high and low foam qualities (injected gas volume fraction) (Fig. 1) (Alvarez *et al*., 2001). The high-quality regime is controlled by lamella stability, while in the low-quality regime foam lamellae are relatively stable, bubble size is fixed, and behavior is controlled by gas trapping and mobilization. In the high-quality regime, water saturation S_w is held nearly constant at the water saturation S_w^* corresponding to the "limiting capillary pressure" (Khatib *et al*., 1988; Rossen and Zhou, 1995). In the high-quality regime, applying Darcy's law to the aqueous phase at fixed water saturation S_w^* gives

$$\nabla p = u_w \mu_w / (k\, k_{rw}(S_w^*)) \qquad (1)$$

where u_w is water superficial velocity, μ_w is aqueous-phase viscosity, k is permeability and $k_{rw}(S_w^*)$ the relative permeability to the aqueous phase at S_w^*. Our hypothesis is that polymer affects foam in the high-quality regime by (a) viscosifying the aqueous phase (increasing μ_w) and (b) stabilizing or destabilizing foam lamellae (reducing or increasing S_w^*, respectively). One can distinguish between these effects by measuring the viscosity of the aqueous phase separately from the foam (accounting if possible for the effects of shear rate on polymer viscosity). If upon addition of polymer the pressure gradient in porous media in the high-quality regime increases more than does μ_w, then polymer stabilizes foam lamellae (reduces S_w^* and k_{rw}); if pressure gradient increases less than does μ_w, then polymer destabilizes the lamellae (raises S_w^* and k_{rw}). If measured ∇p data are in the low-quality regime, then the relation between $k_{rw}(S_w)$ and foam stability is less direct, but one would still expect ∇p to reflect water saturation and water viscosity, and one can separate the effects of polymer on each.

Characterizing foam behavior in a plot like Fig. 1 is time-consuming, because it takes many data to make a plot, and each datum may take a one or more days to reach steady-state. In our previous report we showed evidence in some cases of an abrupt jump in foam strength as though a jump between regimes. We did not find further evidence of that behavior in this reporting period, but verifying steady-state continued to be a slow process in some cases.

Our new experiments were conducted in a 3.67-darcy sandpack. The surfactant is a 0.39 wt% active (1 wt% as received) solution of Bio-Terge AS-40 (an alpha olefin sulfonate), manufactured by Stepan Chemical Co., in brine with 0.25 wt% NaCl and 0.01 wt% $CaCl_2$. Back-pressure was about 600 psi and nitrogen was the gas. In other respects, the coreflood apparatus was similar to that in previous reports. Polymer-foam solutions for this period included 0.05 wt% of xanthan polymer (Xanvis, from Kelco Oil Field Group) (MW~5-7,000,000) in the surfactant formulation. The viscosity of the aqueous foam formulation with polymer (but without gas) was 4.6 cp. (It varies slightly from one batch to another; in our last report, we cited a value of 3.9 cp for this same formulation.)

One goal of this work is to examine the effect of oil on foam both with and without polymer. We use decane as the oil, because in separate tests decane appeared to destabilize bulk foam made with our surfactant formulation more effectively than did the crude oils we had on hand. For tests with oil, we follow here the procedure of Mamun *et al*. (2002). Oil is displaced from sandpacks by high pressure gradients. Therefore, to produce reproducible, fairly constant conditions with oil present (and to ensure that oil *is* present in significant amount), we inject oil along with the foam at a fixed volume fraction of injected fluids. In this case the injected oil volume fraction is 22%.

Fig. 2 shows behavior with no polymer and no oil in a 3.67 darcy sandpack. Fig. 3 shows behavior with decane but no polymer. The data in Fig. 3 appeared in our previous semi-annual report. Decane reduces the pressure gradient with foam moderately here, i.e. by about 30-40%. In our previous report we showed a comparison in a 16.6 darcy sandpack in which decane drastically reduced pressure gradient with foam. In that same report we show a comparison in 16.6 darcy rock that suggests that without oil, polymer increases the foam pressure gradient, but by a factor less than it increases the viscosity of the aqueous formulation alone. This suggests that polymer destabilizes foam slightly, raising water saturation S_w and water relative permeability k_{rw} (Eq. 1), but the increase in the viscosity of the aqueous phase more than compensates in the pressure gradient.

Fig. 4 shows the same system with decane and with xanthan polymer in the foam formulation. Pressure gradient is actually a little lower than without polymer. *Polymer did not stabilize foam in the presence of decane*. In fact, given that the aqueous phase is 4.6 times as viscous in Fig. 3 than in Fig. 2, polymer must have destabilized foam, reflected in a rise in water saturation and water relative permeability (Eq. 1).

Fig. 5 shows the behavior of foam without polymer or oil injected along with the foam in the same sandpack as the preceding figures, after that sandpack had contacted both polymer and oil. Evidently some oil remains in the pack; the pressure gradient is less than in Fig. 1. Thus foam is sensitive to even the relatively small residual oil saturation in this sandpack at high pressure gradient.

Experiments of foam with oil and polymer are continuing.

TASK 2: GAS TRAPPING

Our efforts on this task were boosted by the arrival in late fall of Dr. Quoc Nguyen, who had just completed his PhD in Petroleum Engineering at the Technical University of Delft in The Netherlands. A significant part of Dr. Nguyen's PhD dissertation concerned gas trapping and gas-phase tracer experiments with foam

Tracer Experimental Apparatus

During this period we completed construction and testing of an apparatus for measuring flowing-gas fraction in foam corefloods using gas-phase tracers. It is essentially a conventional coreflood apparatus with a gas chromatograph (g.c.) as close as possible to the outlet of the core. One of the trickiest aspects of such experiments is breaking the foam and separating the surfactant solution before gas enters the chromatograph, while minimizing the apparatus volume downstream of the core. We accomplished this by injecting a small amount of methanol just upstream of a T in the line. The methanol effectively breaks the foam and causes the liquid to drain downward at the T, while gas rise upwards to enter the g.c..

Fig. 6 shows reproducibility in two experiments with flow through a foam generator, using N_2 for the foam and 10% He as the tracer. The surfactant was Shell Neodol 25-9, a nonionic surfactant used earlier by Jisung Kim in our group (Kim *et al*., 2004). The reproducibility between the two runs is excellent, and surfactant was prevented from entering and damaging the g.c.. The data illustrate the difficulty in accurately resolving the late portion of the tracer breakthrough curve, however, due to scatter in the data. The gaps in data are caused by the need to briefly pause the data-acquisition process periodically for downloading data. We are examining ways to work around this problem. The gaps are not significant if the front takes a longer time to come through, as illustrated in Fig. 7. This figure shows the breakthrough curve for tracer in a Berea core sample with no foam present.

Inferring Trapped-Gas Saturation from Tracer Breakthrough Curves

Until Dr. Nguyen's PhD research at the Technical University of Delft, the state of the art for determining trapped-gas saturation was the approach of Gillis and Radke (1990). They injected foam into a core until steady state was reached, and then injected a tracer. Any study of tracer transport though foam must confront the reality that tracer can diffuse through foam films and enter trapped gas bubbles. Thus the tracer breakthrough curve is distorted by dispersion along the flowing path and diffusive mass transfer back and forth with the trapped bubbles.

Gillis and Radke assumed first that the flowing fraction is a static, distinct portion of the foam. They further assumed that the trapped gas has a concentration of tracer, gained by diffusive mass transfer with the flowing gas, that is uniform across each core cross-section, with the mass-transfer rate governed by an effective mass-transfer coefficient. In other words, there is resistance to transfer of tracer from the flowing gas to trapped gas, but instantaneous transport of this tracer throughout the trapped gas at that axial position along the core. The flowing-gas fraction is then determined by a model fit to tracer breakthrough data. Close examination of the results shows that in some cases most of the delay in tracer breakthrough is caused by mass transfer with trapped gas, not directly by the trapped or flowing gas fractions. In other words, the inferred flowing gas fraction is sensitive to the assumptions of and fit to the mass-transfer model.

Friedmann *et al*. (1991) did not attempt to model mass transfer with trapped gas explicitly in their experiments. They simply assumed that the leading portion of the

tracer breakthrough curve represents where tracer would have broken through if not delayed by mass transfer with trapped bubbles.

Direct Observation of Tracer Through CT Imaging

In his PhD research at the Technical University of Delft (TUD), Dr. Nguyen performed experiments with a CT scanning and Xe, a gas-phase tracer that is visible in CT. An example result is shown in Fig. 8, from. Nguyen's dissertation (2004). In this case, foam flows at steady state through a small Bentheim sandstone core before a portion of the gas phase is replaced with Xe. The surfactant concentration is low in this experiment, and there is no back-pressure on the core. Details are in Nguyen's dissertation (2004). In addition to his CT tracer studies, Nguyen measured the diffusion rate of tracer through foam films. To quantify the trapped-gas fraction from his CT images, he tracked the concentration in each voxel as a function of time. Nguyen estimated the fraction of flowing gas in each voxel as the fraction of a normalized concentration of 1 achieved in an initial, rapid rise, which he took to be due to convection. The remaining, slower rise in concentration he took to be diffusion into trapped gas in the voxel. In that way, Nguyen obtained an estimate of the trapped and flowing gas fractions in each voxel. Summing over all voxels gave an estimate of trapped and flowing fractions in the core.

Through arrangement with the research program at TUD, we are continuing the analysis of these data. For instance, Fig. 9 shows cross-sectional images reconstructed from the axial CT data at three times. It is immediately clear that tracer is convected through these cross-sections at a relatively small number of locations and then diffuses outwards from these locations. The concentration of tracer is not nearly uniform in the trapped gas phase, as assumed in earlier modeling.

For comparison with Nguyen's original analysis, we plan a separate evaluation of trapped-gas saturation from these data as follows:

1. Using Nguyen's diffusion measurements, develop a simple model for gas diffusion trough trapped foam. In other words, derive an effective diffusion coefficient for tracer through trapped foam of some representative bubble size.
2. Combine this effective diffusion coefficient with solutions for unsteady diffusion Bird *et al*., 2002) to estimate distances over which tracer would be expected to diffuse over a given period. Use this estimate to calibrate the analysis in the following steps.
3. In the cross-sectional images, divide the images into flowing and trapped gas as follows: (a) Assume that any local maximum in tracer concentration represents a location where tracer flows into the cross-section, i.e. flowing gas. (b) Assume regions between local maxima where tracer concentration rises reflects tracer diffusion from those other regions where tracer is flowing. (c) Regions with negligible tracer concentration reflect trapped gas. (d) An exception to (a) is a local maximum where the value of tracer concentration is decreasing, as occurs occasionally. Assume this represents a region where tracer once flowed, but convection has stopped, and tracer is diffusing away into surrounding trapped gas. Use the results of (2) to inform this analysis; if diffusion is inferred over distances too large to be reasonable over the time frame assumed, then reject diffusion as an explanation for the rise in tracer concentration, and assume it is convection instead.

Using this method, we can obtain an independent measure of trapped-gas saturation from the CT data, for comparison with other estimates.

Nguyen did not measure the tracer breakthrough curve in these experiments. One can reconstruct the curve from the images by conducting a mass balance on tracer in the core. We plan to do so, and then use the modeling approach of Gillis and Radke (1990) to estimate trapped and flowing gas from this curve. Possible refinements to this approach include using solutions for unsteady diffusion into trapped gas (Bird *et al*., 2002) rather than assuming a fixed mass-transfer coefficient and uniform concentration within the trapped gas. Then the three estimates of flowing gas - Nguyen's original analysis, our analysis based on cross-sections, and the modeling of Gillis and Radke - will be compared.

Nguyen's experiments were limited to low surfactant concentration, no back-pressure, relatively weak foam, and short core. Once we have identified the most accurate way to interpret breakthrough curves through comparison with Nguyen's CT data, we will use that approach to analyze our tracer data for strong foams in 1-ft cores with back-pressure. We are also investigating possible imaging experiments using an NMR facility in our Department or by collaboration with TUD or others.

TASK 3: FOAM GENERATION

We continue experiments examining foam generation with limited pressure gradient, following up on earlier research showing a minimum pressure gradient for foam generation and an unstable regime at intermediate pressure gradients (Gauglitz *et al*., 2002; Kam and Rossen, 2002). Our experiments are conducted in sandpacks; the same trends in foam behavior are observed in sandpacks as in consolidated core, but at lower pressure gradient (Khatib *et al*., 1988; Alvarez *et al*., 2001; Gauglitz *et al*., 2002). It is much more convenient to work in sandpacks than consolidated core, because at low pressure drop in a sandpack one does not need to apply back-pressure. Fluctuations in back-pressure are hard to completely eliminate, and they can introduce transient false pressure gradients into the apparatus, which can in turn trigger foam generation. The lack of elevated back-pressure does mean that gas compression can affect gas flow rate near the inlet at high pressure drops across the core. Gas flow rates are measured (though not controlled) by a Brooks Instruments Co. mass-flow controller. Pressure drop across the core is set by a conventional pressure regulator in the gas line. All experiments reported here were conducted with Bio-Terge AS-40 surfactant.

Experiments in this period focused on foam generation in flow across layer boundaries. In all cases sandpacks were prepared with a lower-permeability region upstream, and an abrupt transition to a higher permeability about midway through the pack. In all cases, the increase in permeability was by a factor of at least four, which modeling suggests should be sufficient to trigger strong-foam generation (Ransohoff and Radke, 1988; Falls *et al*., 1988; Rossen, 1999). In all cases the pack is held vertically and fluids are injected from the top of the pack.

Steady-State Experiments

First, following the approach of Gauglitz *et al*. (2002), we conducted experiments with fixed liquid injection rate and fixed pressure drop across the core, with the following procedure: The sandpack is initially saturated with brine. Then gas and brine are injected until steady state is achieved. Surfactant solution and gas are then injected at the same rates as brine and gas, for a sufficient period for surfactant solution to replace the brine in the sandpack at a pressure gradient too low to create foam. Then pressure drop on the gas line is raised in a series of steps, while holding liquid injection rate fixed. Gauglitz et al. use this sort of experiment to demonstrate the existence of three foam

states: a coarse foam state with high gas flow rate and high gas mobility; an intermediate state in which gas flow rate decreases as pressure gradient increases, or the pack is plugged; and a strong-foam state where pressure gradient is high and gas flow rate starts again to increase with increasing pressure gradient.

Fig. 10 shows the results with a sandpack of 8.5 darcy upstream and 41.1 downstream, for a jump of 4.8 in permeability at a location within section 2 (out of four) in the pack. Behavior is similar to that in Gauglitz *et al*. (2002) for a homogeneous pack, except that the pack remains nearly plugged at the maximum pressure gradient. Fig. 11 shows the sectional pressure drops in this experiment; the lower-case letters in both figures correspond to the same points. In the coarse-foam regime (pts. a and b), most of the pressure drop occurs in the first section of the core, near the inlet. At the transition from coarse foam to the intermediate state (b to c), most of the pressure drop now occurs in section 2, where the transition in permeability is located and foam generation is expected. As in Gauglitz *et al*., in the intermediate state the flow rate in the core is not constant in time; in particular, when nearly plugged, the core alternates between a bursts of flow and plugging. At higher pressure drop (pt. d), some foam evidently has been displaced into the third section, and the total pressure drop is now shared between sections 2 and 3. At still higher pressure drop (not shown), there is significant pressure drop in sections 1, 2 and 3, but not 4. One might conjecture that the core will remain plugged at yet-higher pressure drop until foam has propagated through section 4 and reached the end of the core.

Fig. 12 shows results from a similar experiment, with a lower liquid injection rate. Foam generation is triggered at a lower pressure drop across the core than in Fig. 10.

As we have discussed in previous reports, it is hard to interpret pressure-drop data alone in terms of coarse or strong foam. Fig. 13 shows the effective gas relatively permeability in both experiments, averaged over the sandpack, and lumping all resistance to gas flow into the relatively permeability. Where the core appears to be plugged (pressure gradient greater than 2 psi/ft), the gas mobility is indeed greatly reduced by foam.

Dynamic SAG Displacements

Next we examined foam generation during gas injection into a beadpack saturated with surfactant solution (a "SAG" displacement). Again, pressure drop was held fixed rather than (gas) injection rate. In this case the permeability contrast within the beadpack was extreme: 1.2 darcy upstream and 97.8 darcy downstream. In this case there were five sections to the beadpack, and the transition in permeability was in section 3.

Fig. 14 shows the results for a pressure drop of 8.5 psi. and 0.1 wt% surfactant concentration. Behavior is complex. At the start, all pressure drop is in section 1, but this pressure drop falls rapidly as pressure drop rises in section 2. Pressure drop falls in section 2 as it rises in section 3. Foam generation evidently occurs in section 2, as gas flow rate Qg reaches a minimum, but soon most of the resistance to flow in the pack is in section 3. Gas flow rate rises slowly in time. The foam evidently is does not propagate to section 4, which never shows a significant pressure drop.

Fig. 15 shows similar results for an experiment with a lower pressure drop, 4 psi, across the beadpack. Results are qualitatively similar to Fig. 14. Fig. 16 shows a case similar to Fig. 14 but with 1 wt % surfactant rather than 0.1 wt %. Again, the results are qualitatively similar.

Behavior appears to be shaped by whether or not foam is convected forward or remains trapped in the given core section. This leads us to consider the roles of foam

generation and convection in foam propagation, which will be a focus of work in the next semi-annual period.

Foam Displacements With Abrupt Changes in State

Foam generation is a phenomenon in which the flow of gas and liquid in a porous medium undergoes an abrupt change of regime. In conventional experiments with gas and liquid injected simultaneously at fixed rates, the onset of foam generation can change the pressure drop across a core by a factor of tens or hundreds in a matter of minutes. On a field scale, this change is essentially instantaneous, and it would be modeled as an abrupt jump between two possible steady-state regimes. Foam generation then is an abrupt jump from a state of no-foam or coarse foam to a state of strong foam. There is limited evidence of a corresponding jump from strong foam to coarse foam as foam dries out at the limiting capillary pressure.

Furthermore, there is some evidence that the capillary-pressure function $P_c(S_w)$ may differ between these foam regimes. In particular, because in a strong foam some water is occupied in separating the gas bubbles, there is less water to occupy narrow pores; as a result, one would expect that at the same water saturation S_w, $P_c(S_w)$ would be higher in a strong foam than a coarse foam. There is some evidence for this (Khatib *et al*., 1988; Kibodeaux and Rossen, 1997), but it is not clear how large an effect this would have in consolidated porous media.

In collaboration with J. Bruining of the Technical University of Delft, we investigated the implications of these abrupt changes on SAG foam displacements, i.e. displacements where gas and liquid are injected in alternating slugs. For calculations, we used a hypothetical local-steady-state foam model with two steady-state foam regimes, "strong foam" and "no foam." This model is illustrated in Fig. 16. If there is no foam initially in the core, then the core is in the "no-foam" state. The no-foam regime reaches its limit at $S_w = 0.7$ (water fractional flow $f_w = 0.00999$), at which point no-foam abruptly reverts to strong foam (i.e. foam generation occurs). The strong-foam regime reaches its limit at $S_w = 0.37$ ($f_w = 0.0075$), at which foam abruptly reverts to no foam (i.e. remaining foam collapses). The strong-foam and no-foam behavior in this model is roughly consistent with that reported by Persoff *et al*. (1991), who found strong-foam behavior down to the limit of that study, $f_w = 0.004$. The jump between regimes is a conjecture added here for illustration. If there were a jump in the foam studied by Persoff *et al*., it would occur at $f_w < 0.004$, lower than we assume here for illustration.

In addition, for some calculations we assume that when strong foam is present, the $P_c(S_w)$ function is 50% greater than the function that applies to "no-foam," as suggested by some studies. In other cases, the $P_c(S_w)$ function was the same for both states.

Rossen and Bruining (2004) present evidence supporting these conjectures and show the implications for foam displacements using fractional-flow theory and computer simulations. Their conclusions are as follows:

1. A number of experimental and theoretical studies suggest that the fractional-flow function $f_w(S_w)$ for some foam processes is either multi-valued in S_w or else comprises distinct fractional-flow curves for two or more foam regimes, with jumps between them when each regime reaches its limiting condition. Fig. 17 shows an example from Kibodeaux and Rossen (1997).
2. If the predicted or measured fractional-flow function includes portions where $(df_w/dS_w) < 0$, as in Fig. 17, these portions of the fractional-flow functions do not

represent possible homogeneous steady-states and cannot be present within spreading waves with positive velocity. Any region at such a saturation, if present, would spontaneously split into zones of higher and lower saturation. In a displacement, such a fractional-flow function would behave as a system with two distinct fractional-flow functions, as illustrated in Fig. 16.

3. In cases with two distinct fractional-flow functions, the solution for a given displacement begins with consideration of the path of saturations that would be present in the traveling wave at the shock: in particular, equal capillary pressure at the jump between regimes. This leads one to identify the portions of the fractional-flow function that apply to the given displacement. Once one identifies the relevant portions of the fractional-flow curve, the standard graphical methods of fractional-flow analysis (Zhou and Rossen, 1995; Rossen *et al*., 1999; Shan and Rossen, 2004) apply.
4. Differences between capillary-pressure functions for strong foam and coarse foam or no-foam are plausible and have experimental support. If such differences exist, they can exert a strong influence on field-scale displacements. For the data of Kibodeaux and Rossen (1997), an additional broad region of constant state is introduced, with much-different mobility control than with no difference in capillary pressures between strong foam and weak foam. It is therefore important to determine experimentally whether capillary pressure in porous media depends on the existence and state of the foam present. Figs. 18 and 19 show computed results for the model in Fig. 16, with and without a difference in $P_c(S_w)$ functions. A broad, low-mobility bank is present in one case that is absent in the other.
5. If one uses experimentally derived transport properties directly, and foam affects the $P_c(S_w)$ function, accurate conventional finite-difference simulation can require extraordinarily large numbers of grid blocks. In one example, an estimated 5000 grid blocks would be required to give an accurate water saturation in the trapped-foam bank in a conventional finite-difference simulation. However, using the effective fractional-flow and capillary-pressure functions appears to eliminate this problem. Simulations with these upscaled functions gave the correct large-scale behavior, with the correct shocks.

Figs. 20 and 21 give the corrected graphical construction of the shock based on the data of Kibodeaux *et al*. (1997) assuming (Fig. 24) that $P_c(S_w)$ is independent of foam strength, and (Fig. 25) that $P_c(S_w)$ is greater for strong foam than coarse foam at the same water saturation.

CONCLUSIONS

Detailed conclusions are listed under each task in the section on Results and Discussion above. Important overall conclusions include the following:

1. Laboratory results so far failed show that decane destabilizes foam. Addition of polymer to the foam formulation did not stabilize foam, however.
2. CT images of gas-phase tracer injected in steady-state foam flow from TU Delft show that the interacting processes of gas convection and mass transfer with trapped gas are much more complex than accounted for in mathematical models to date. We have begun a detailed analysis of these images, combined with a

model for tracer diffusion through trapped bubbles, to estimate the trapped gas fraction in these experiments.

3. Our own laboratory apparatus for determining gas-phase tracer concentrations in effluents is ready for experiments with foam in consolidated core.
4. Foam generation experiments in a heterogeneous sandpack show the same three foam states (coarse foam, strong foam, and intermediate state) as in homogeneous porous media. One implication is that there may be a minimum pressure gradient for strong-foam generation in even heterogeneous porous media.
5. Dynamic SAG displacements in a heterogeneous beadpack show complex dynamics. Pressure rises and falls as a pressure wave moves through the pack. It appears to be crucial whether foam is mobilized and displaced or remains in place.
6. A fractional-flow model for processes with discontinuous jumps in states, like foam generation, has been developed. One must account for the change in saturations within the traveling wave at the shock front. By doing so, one can determine the portions of the fractional-flow curves for the various states that applies to a given displacement. Once this is done, the conventional rules of fractional-flow analysis apply.
7. In a SAG process, it can be crucial whether strong foam has a different capillary pressure than coarse foam at the same water saturation. There is limited evidence that capillary pressure does depend on foam strength. If so, then SAG displacements can show an extra foam bank and improved mobility control.

REFERENCES

Alvarez, J. M., Rivas, H., and Rossen, W. R.: "A Unified Model for Steady-State Foam Behavior at High and Low Foam Qualities," *SPE J* (Sept. 2001), 325-333.

Bird, R. B., Stewart, W. E., and Lightfoot, E. N.: *Transport Phenomena*, 2nd ed., Wiley, New York, 2002.

Falls, A. H., Hirasaki, G. J., Patzek, T. W., Gauglitz, P. A., Miller, D. D., and Ratulowski, J: "Development of a Mechanistic Foam Simulator: The Population Balance and Generation by Snap-Off," *SPERE* (Aug. 1988) 884-892.

Friedmann, F., Chen, W. H., and Gauglitz, P.A.: "Experimental and Simulation Study of High-Temperature Foam Displacement in Porous Media," *SPERE* (Feb. 1991) 37-45.

Gauglitz, P.A., Friedmann, F., Kam, S. I, and Rossen, W.R., "Foam Generation in Homogeneous Porous Media," *Chem. Eng. Sci.* **57***,* 4037-4052 (2002).

Gillis, J. V., Radke, C. J.: "A Dual Gas Tracer Technique for Determining Trapped Gas Saturation During Steady Foam Flow in Porous Media," paper SPE 20519 presented at the 1990 SPE Annual Technical Conference and Exhibition, New Orleans, Sept. 23-26.

Kam, S. I., and Rossen, W. R., "A Model for Foam Generation in Homogeneous Porous Media," paper SPE 77698, presented at the SPE 2002 Annual Technical Conference and Exhibition, San Antonio, 29 Sept. - 2 Oct; accepted for publication in *SPEJ*.

Khatib, Z.I., Hirasaki, G.J., and Falls, "Effects of Capillary Pressure on Coalescence and Phase Mobilities in Foam Flowing Through Porous Media," *SPERE* (Aug. 1988), 919-926.

Kibodeaux, K.R. and Rossen, W.R., "Coreflood Study of Surfactant-Alternating-Gas Foam Processes: Implications for Field Design," paper SPE 38318 presented at the 1997 SPE Western Regional Meeting, Long Beach, CA, June 25-27.

Kim. J. S., Dong, Y., and Rossen, W. R.: "Steady-State Flow Behavior of CO2 Foam," presented at the 2004 SPE/DOE Symposium on Improved Oil Recovery, Tulsa, OK, 17–21 April 2004.

Nguyen, Q. P.: "Dynamics of Foam in Porous Media," PhD dissertation, Technical University of Delft, 2004.

Persoff, P., Radke, C.J., Pruess, K., Benson, S.M., and Witherspoon, P.A.: "A Laboratory Investigation of Foam Flow in Sandstone at Elevated Pressure," *SPERE* (Aug. 1991) 185-192.

Ransohoff, T. C., and Radke, C. J.: "Mechanisms of Foam Generation in Glass-Bead Packs," *SPERE* (May 1988), 573-585.

Rossen, W.R., "Foam Generation at Layer Boundaries in Porous Media," SPE Journal (Dec. 1999), 409-412.

Rossen, W. R., Zeilinger, S. C., Shi, J.-X., and Lim, M. T., "Simplified Mechanistic Simulation of Foam Processes in Porous Media," *SPE Journal* (Sept. 1999), 279-287.

Rossen, W. R. and Zhou, Z. H.: "Modeling Foam Mobility at the Limiting Capillary Pressure," *SPE Adv. Tech*. **3**, 146 (1995).

Shan, D. and Rossen, W.R., "Optimal Injection Strategies for Foam IOR," paper SPE 75180 prepared for presentation at the 2002 SPE/DOE Symposium on Improved Oil Recovery, Tulsa, OK, April 13-17; *SPE Journal*, in press.

Zhou, Z.H. and Rossen, W.R,. "Applying Fractional-Flow Theory to Foam Processes at the 'Limiting Capillary Pressure'," *SPE Adv. Technol*. **3**, 154-162 (1995).

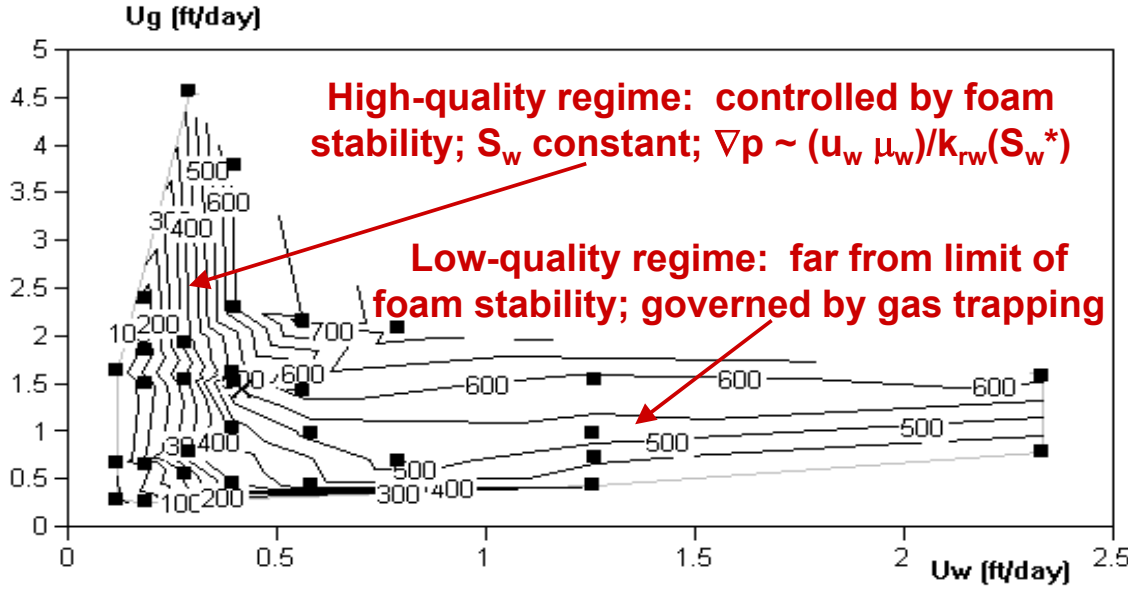

Fig. 1. Steady-state pressure gradient as a function of superficial velocities of gas (U_g) and water (U_w) for one N_2 foam formulation in a Berea core, from Alvarez *et al.* (2001), illustrating the two conventional steady-state strong- foam regimes. Dark dots represent individual data.

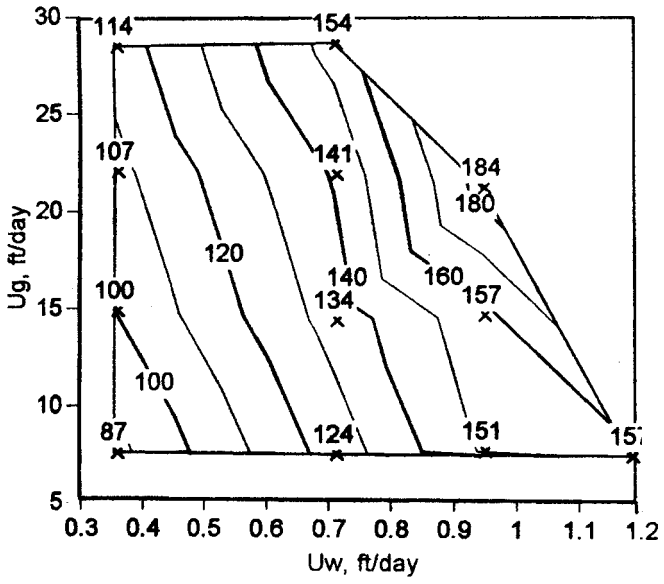

Fig. 2. Steady-state pressure gradient as a function of superficial velocities of gas (U_g) and water (U_w) for N_2 foam without decane or polymer in a 3.67-darcy sandpack. X symbols represent individual data, and the numbers above them the measured values of pressure gradient.

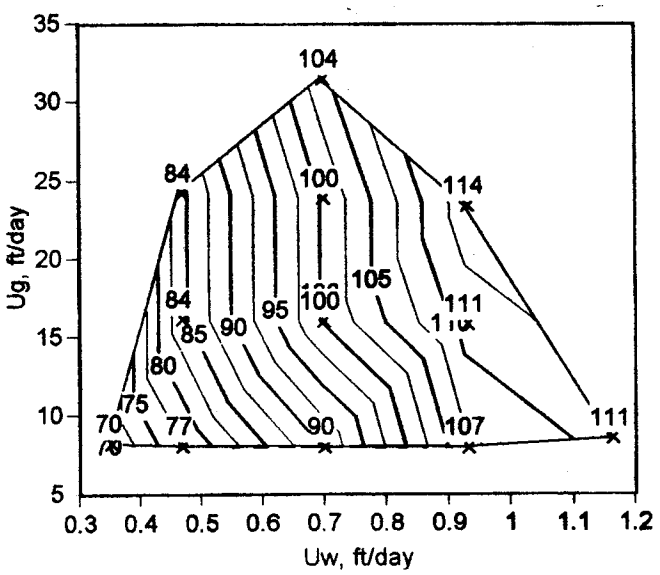

Fig. 3. Steady-state pressure gradient as a function of superficial velocities of gas (U_g) and water (U_w) for N_2 foam with decane but without polymer, in a 3.67-darcy sandpack. X symbols represent individual data, and the numbers above them the measured values of pressure gradient.

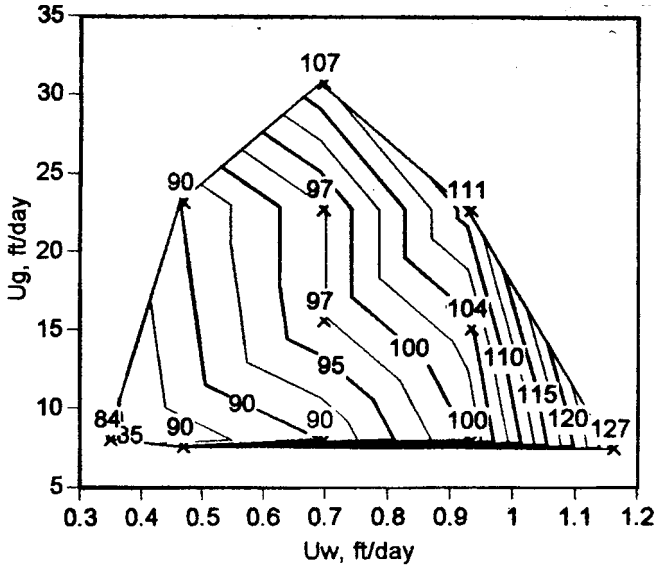

Fig. 4. Steady-state pressure gradient as a function of superficial velocities of gas (U_g) and water (U_w) for N_2 foam with both 0.05 wt%xanthan polymer and 22 vol% decane injected into a 3.67-darcy sandpack. X symbols represent individual data, and the numbers above them the measured values of pressure gradient.

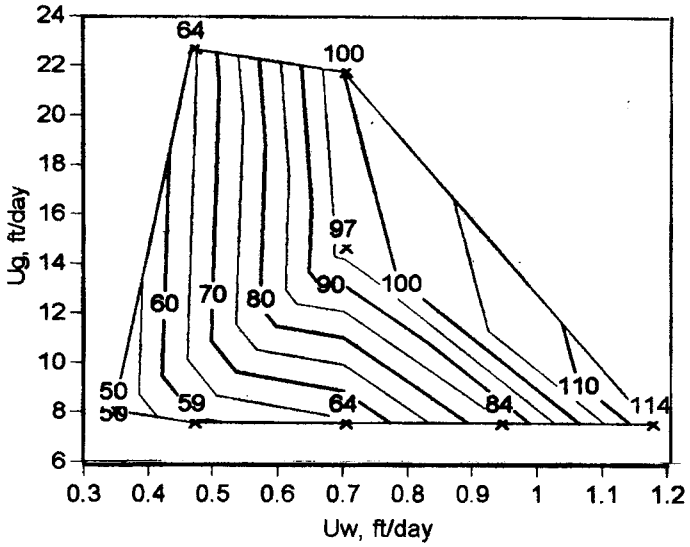

Fig. 5. Steady-state pressure gradient as a function of superficial velocities of gas (U_g) and water (U_w) for N_2 foam without polymer or oil in a 3.67-darcy sandpack, through which polymer and oil have both been injected previous. X symbols represent individual data, and the numbers above them the measured values of pressure gradient.

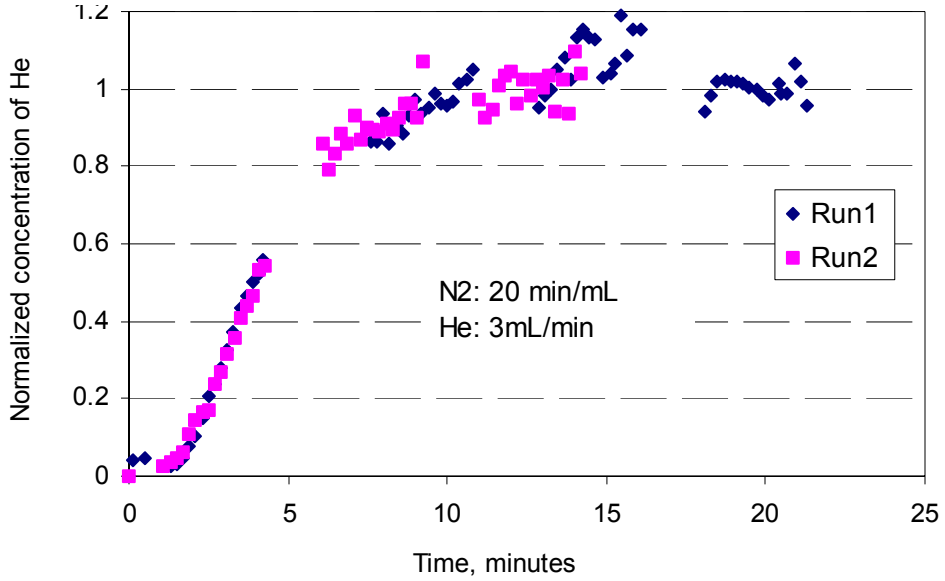

Fig. 6. Reproducibility in tracer breakthrough curve in two experiments with gas and liquid injection through a foam generator.

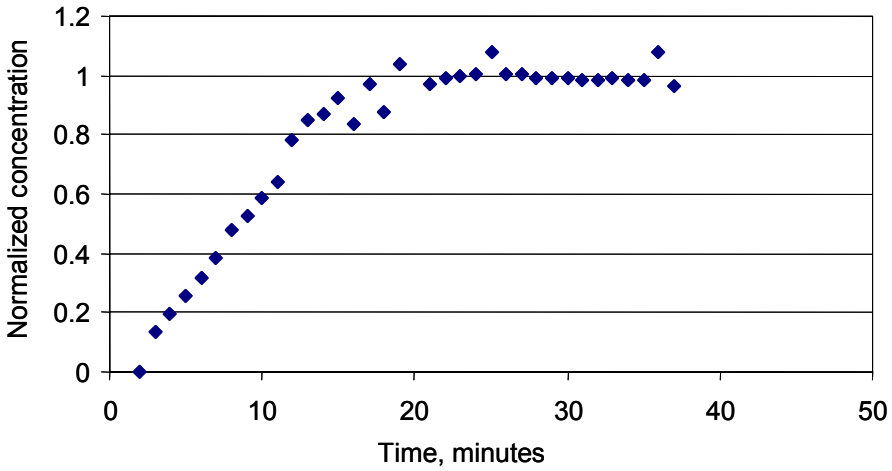

Fig. 7. Tracer breakthrough curve in experiment without foam in a Berea core.

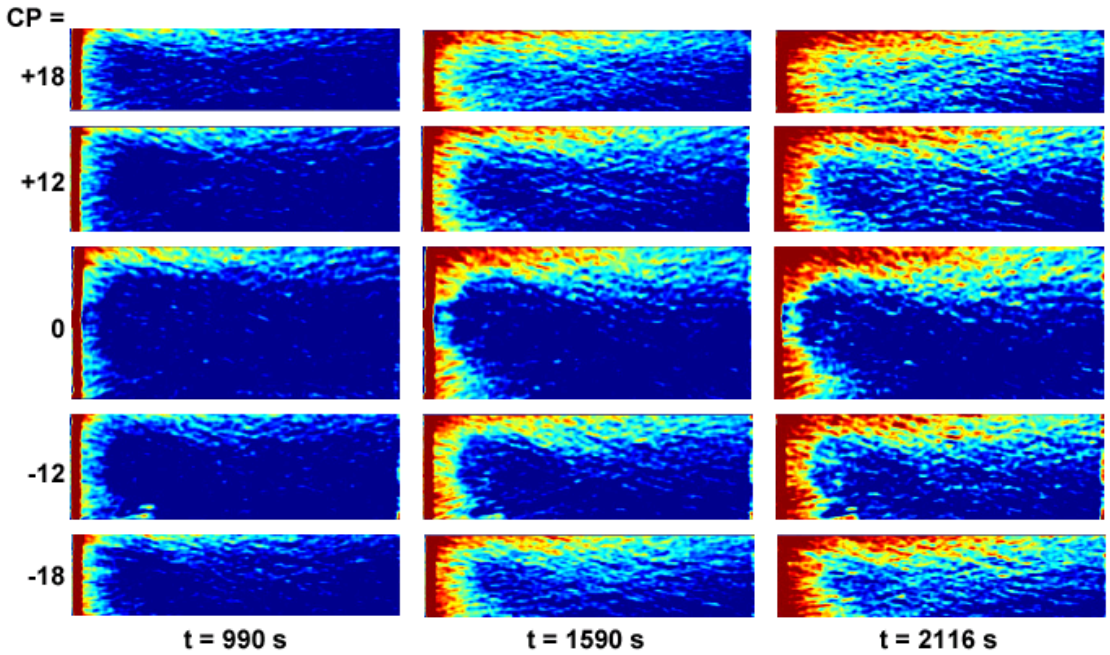

Fig. 8. CT imagines of Xe gas tracer in a Bentheim core. Each row of images corresponds to an axial CT scan along the core, with the central scan in the middle. Each column corresponds to a time after injection of Xe. CT counts per voxel are normalized for local pressure, which is much higher near the inlet than the outlet. Red corresponds to high tracer concentration, dark blue to low concentration. From Nguyen (2004).

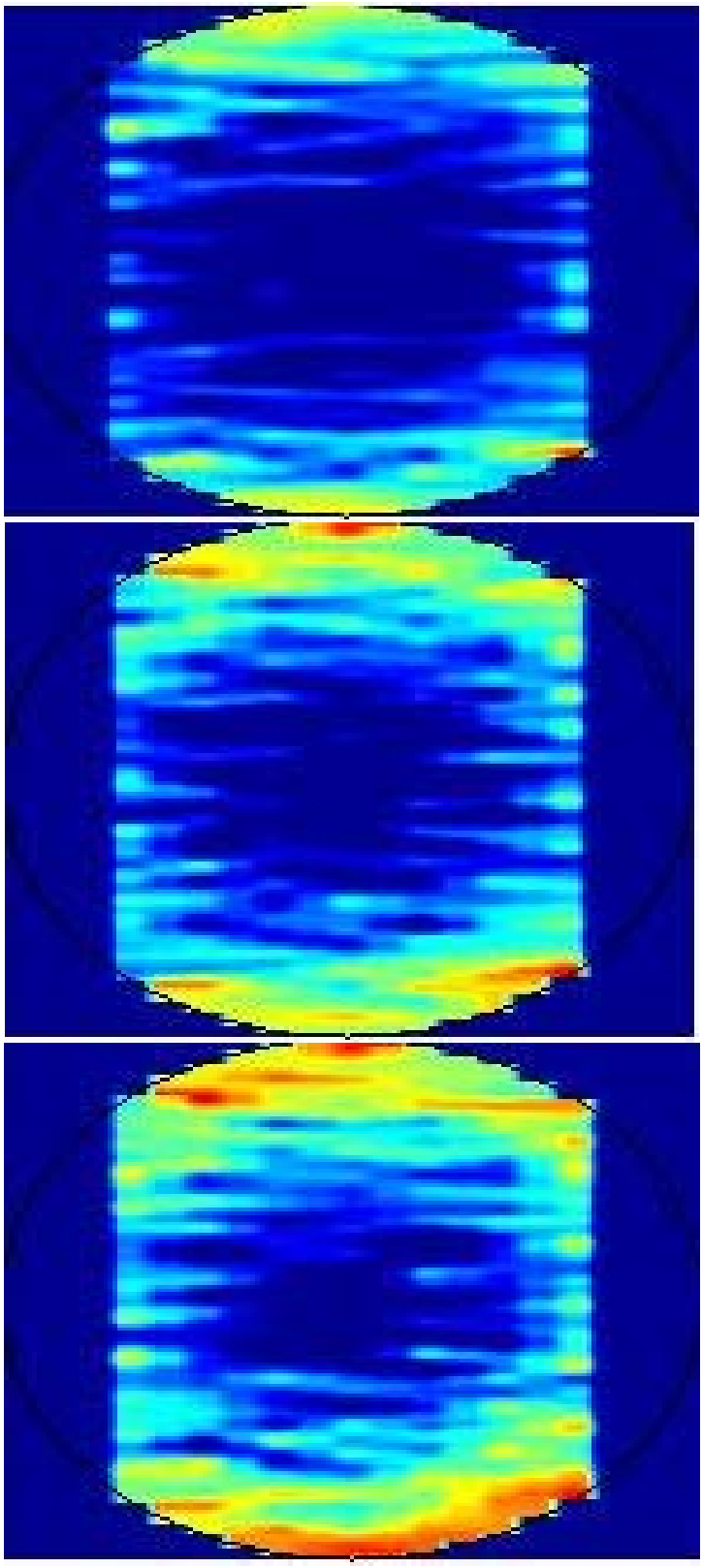

Fig. 9. Cross-sectional image reconstructed from data in Fig. 8; three images at increasing times. Red corresponds to high tracer concentration, dark blue to low concentration.

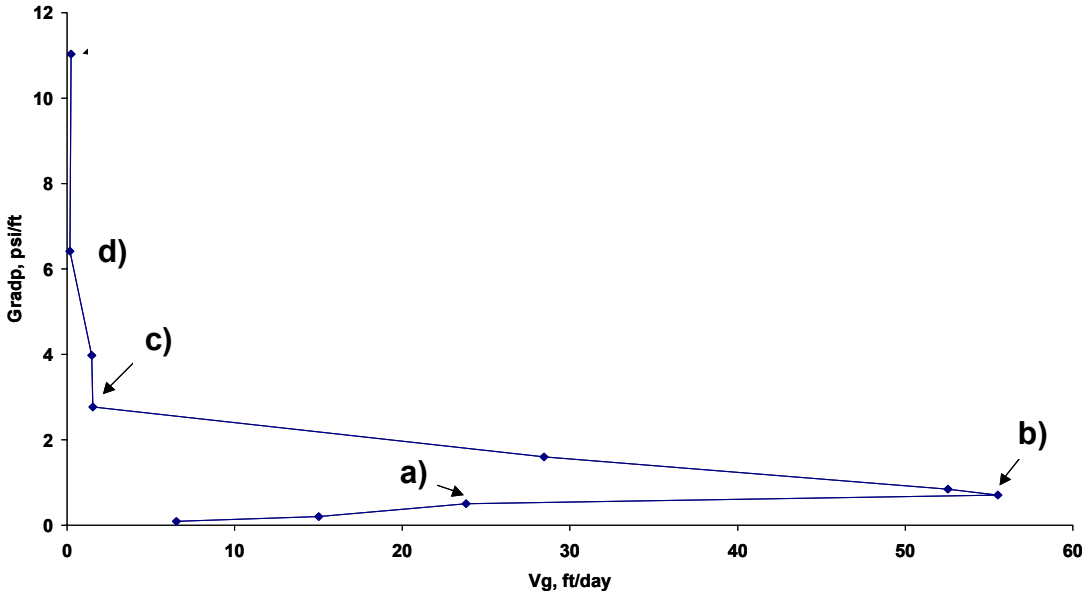

Fig. 10. Gas interstitial velocity as a function of applied pressure drop (averaged here across the sandpack to give an average pressure gradient) across a heterogeneous sandpack. Liquid interstitial velocity is held fixed at 5.24 ft/day, and gas flow is regulated at fixed pressure drop by a pressure regulator upstream of the sandpack. Dots represent steady-state points. Letters refer to plots in Fig. 11.

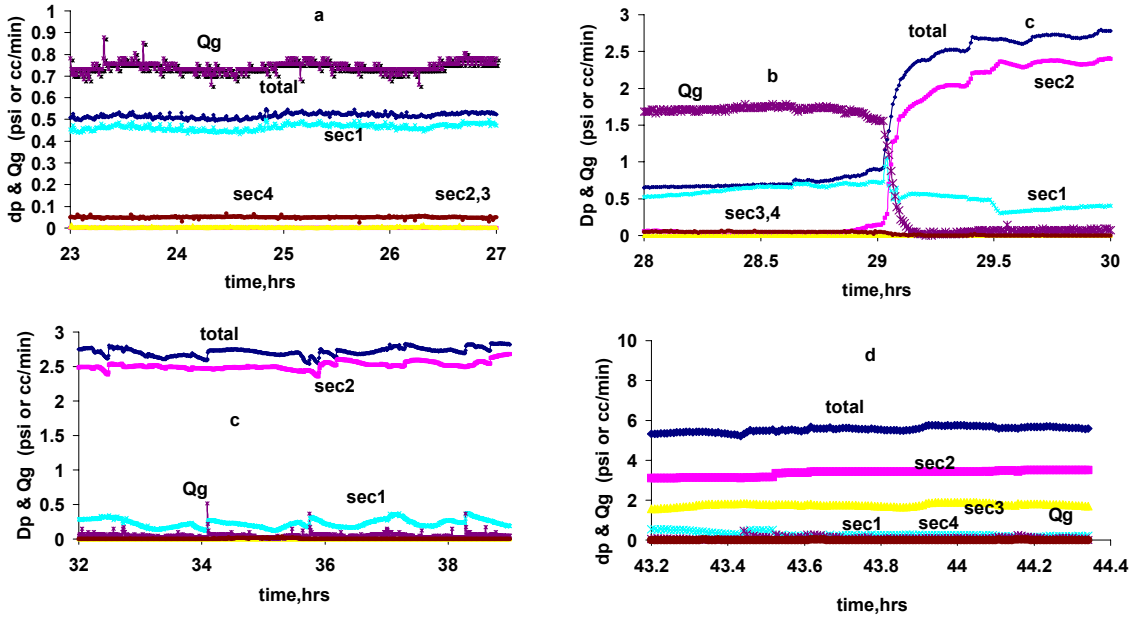

Fig. 11. Gas flow rate, and pressure drop in the individual sections in experiment of Fig. 10.

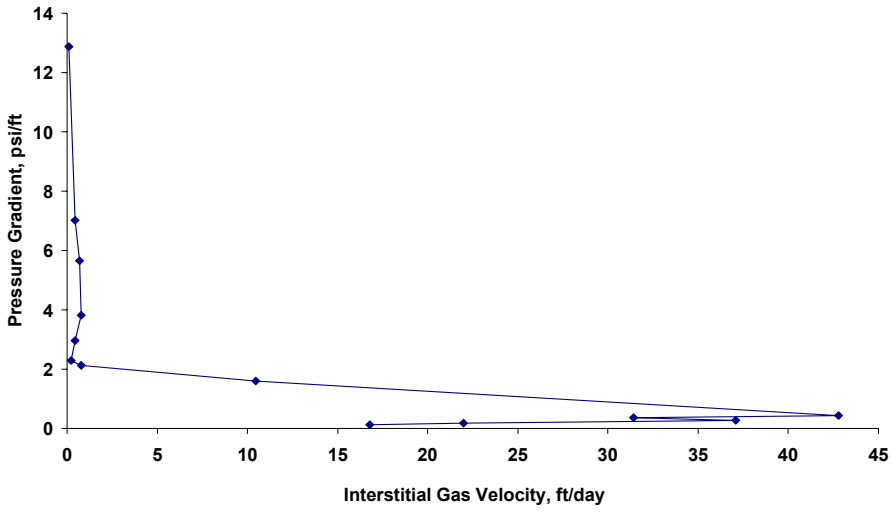

Fig. 3. Pressure Gadient as function of gas interstitial velocity Vg in a Kl/Kh=8.5/41.1 sand pack; 1 wt% surfactant; liquid interstitial velocity Vw=3.49ft/day

Fig. 12. Experiment similar to Fig. 10, but with a higher liquid interstitial velocity (3.49 ft/day).

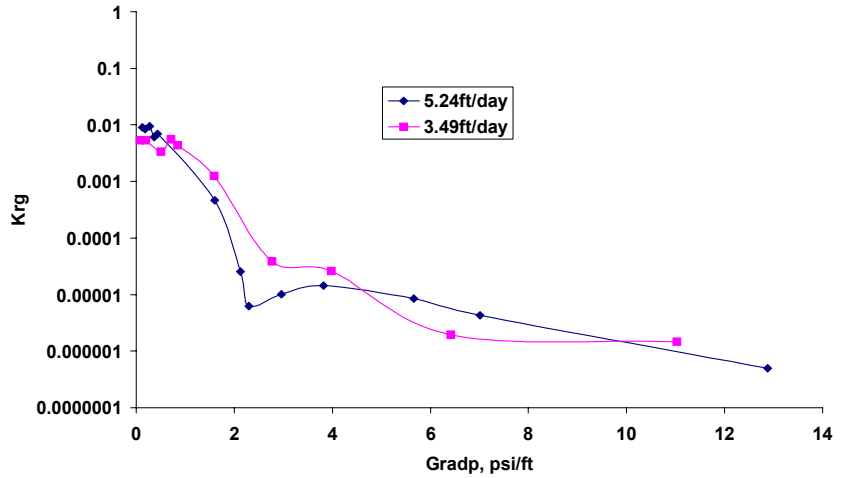

Fig. 13. Effective gas relative permeability for experiments in Figs. 10 and 12.

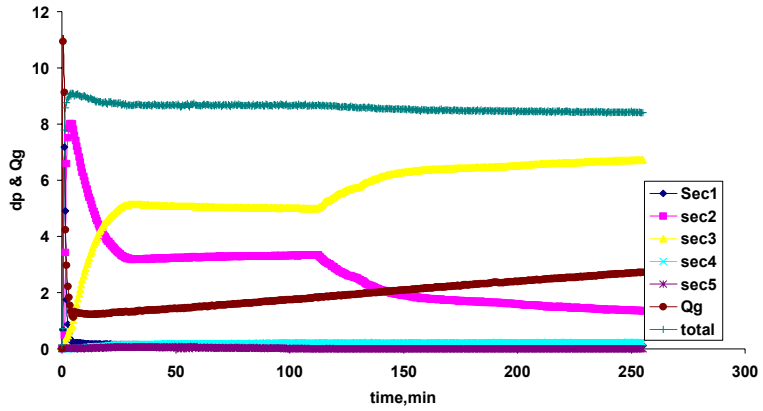

Fig. 14. Sectional pressure drop and gas flow rate in fixed-pressure SAG injection into a beadpack with 1.2 darcy permeability upstream (sections 1 to 3) and 97.8 darcy downstream (sections 3 to 5).

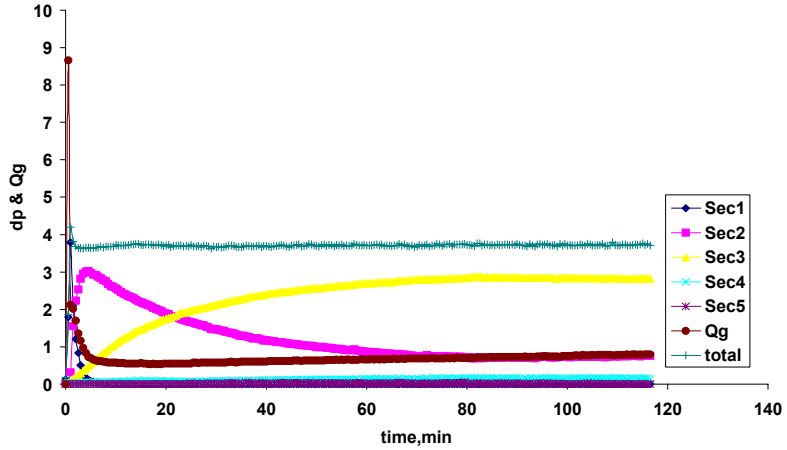

Fig. 15. Result of experiment similar to that in Fig. 14, but with fixed pressure drop of 4 psi across sandpack.

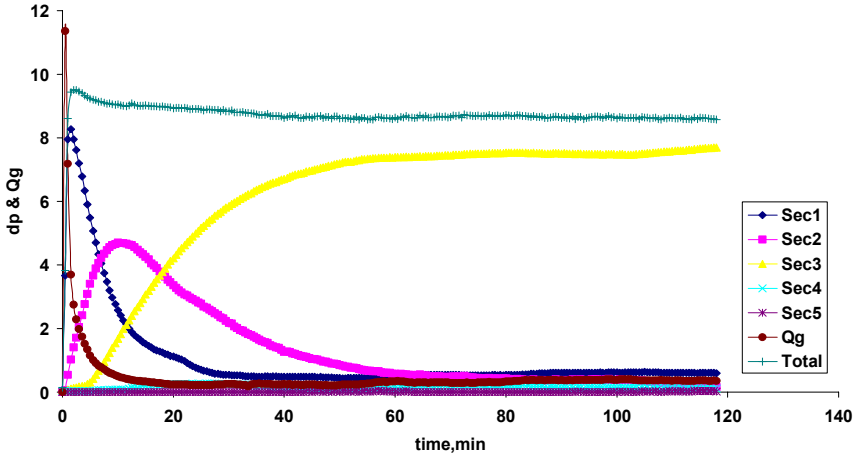

Fig. 15. Result of experiment similar to that in Fig. 14, but with 1 wt% surfactant in aqueous phase.

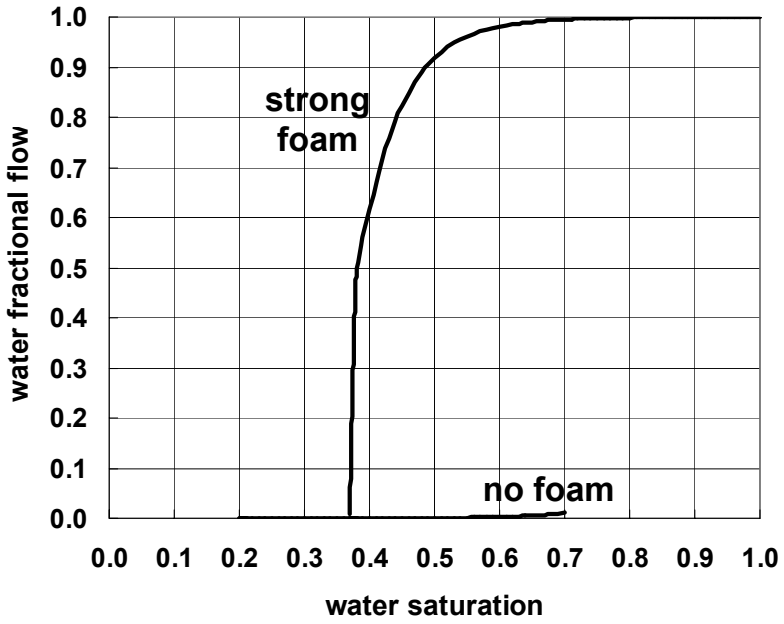

Fig. 16. Foam model used in this study, with two foam regimes, "strong foam" and "no foam." Strong foam reverts to no-foam (foam collapse) if S_w falls below 0.37 (corresponding to the "limiting capillary pressure"); no-foam reverts to strong foam for $S_w > 0.7$ (foam generation). The strong-foam curve ends at $f_w = 0.0075$; there is a jump between curves below this point not obvious on this scale. Model details are in Rossen and Bruining (2004).

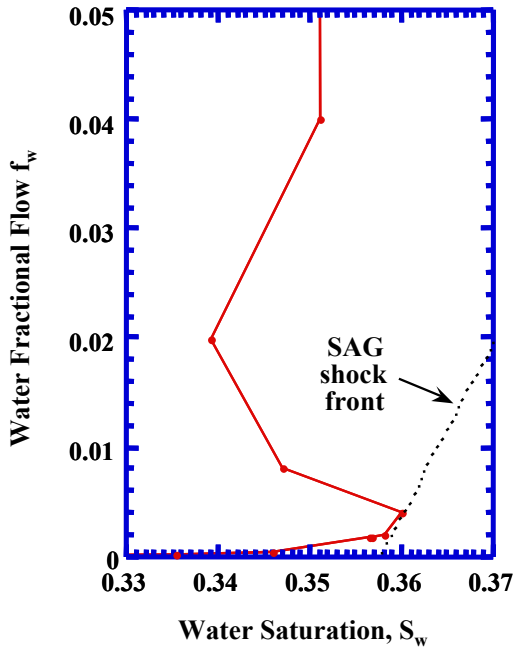

Fig. 17. Experimental $f_w(S_w)$ curve for strong foam from Kibodeaux and Rossen (1997) including shock (incorrectly) suggested by them for SAG displacement.

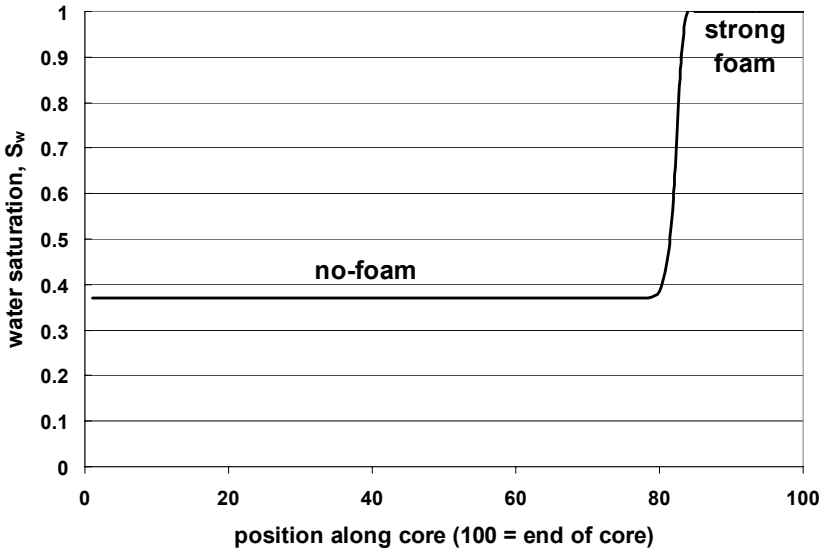

.Fig. 18. Finite-difference simulation of gas injection into a liquid-saturated medium, with no difference in capillary-pressure functions between strong foam and no-foam, after 0.514 PV gas injection. In this case, 100 grid blocks represent a 0.6-m long core. In this example, foam collapses completely at the shock front at the leading edge of the gas bank.

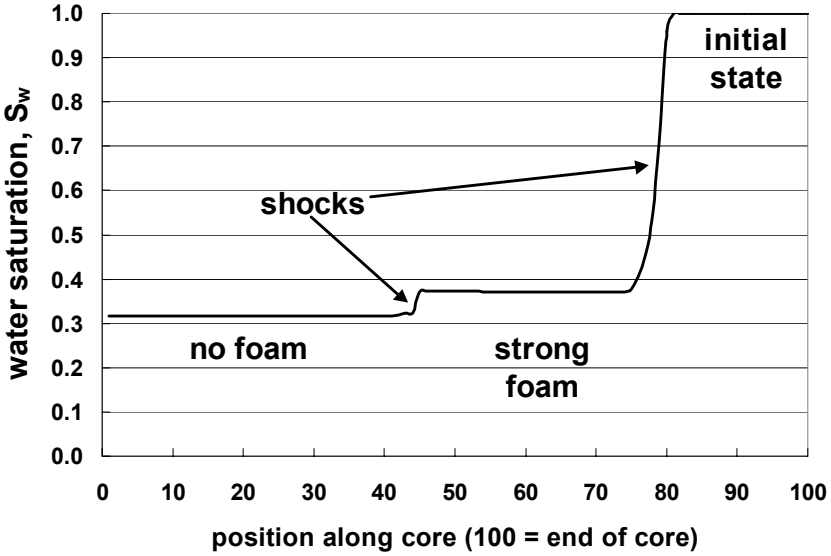

Fig. 19. Finite-difference simulation of gas injection into a liquid-saturated medium, with higher capillary pressure for strong foam, after 0.514 PV gas injection. The only difference with Fig. 18 is that here there is a higher $P_c(S_w)$ function for strong foam than no-foam; this introduces an additional foam bank into the displacement.

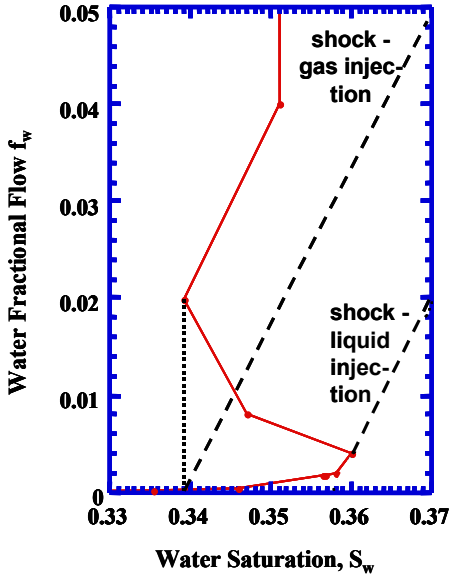

Fig. 20. Revised construction of shocks based on fractional-flow data of Kibodeaux and Rossen (1997) (*cf*. Fig. 17), assuming equal capillary pressure for strong and weak foam. Shock for gas injection would occur to lower portion of fractional-flow curve at same capillary pressure as the lowest-S_w point on the upper portion of curve (just before (df_w/dS_w) reverses sign). This results in poorer mobility control than suggested by Kibodeaux and Rossen based on their graphical construction in Fig. 17. The shock for a process of liquid injection after foam would occur from lower portion of fractional-flow curve to portion of curve at much higher fractional flow (not shown on this scale).

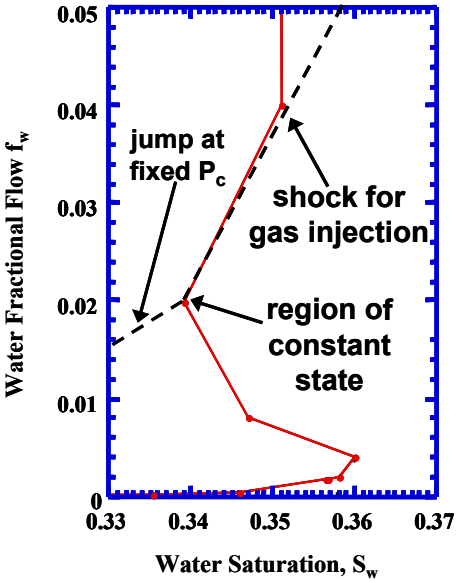

Fig. 25. Revised construction of shock for gas injection based on fractional-flow data of Kibodeaux and Rossen (1997) (cf. Fig. 17), assuming higher capillary pressure for strong foam. In this case there is an intermediate region of constant state of strong foam (*cf*. Fig. 19) at much lower mobility than any bank in Fig. 20. Mobility control would be significantly more effective than suggested by Kibodeaux and Rossen based on their graphical construction, and greatly more effective than suggested by Fig. 20.